Articles in PresS. J Neurophysiol (November 23, 2016). doi:10.1152/jn.00528.2016

Maintenance of neuronal size gradient in MNTB requires sound-evoked activity

Jessica H. Weatherstone[1,2], Conny Kopp-Scheinpflug[3,4], Nadia Pilati[3,5], Yuan Wang[2,6], Ian D. Forsythe[3], Edwin W Rubel[2], Bruce L Tempel[1,2]

[1]Virginia Merrill Bloedel Hearing Research Center, Department of Otolaryngology-HNS, Department of Pharmacology, University of Washington School of Medicine, Seattle, WA
[2]Virginia Merrill Bloedel Hearing Research Center, Department of Otolaryngology-HNS, Department of Physiology and Biophysics, University of Washington School of Medicine, Seattle, WA
[3]Department of Neuroscience, Psychology & Behaviour, University of Leicester, Leicester, LE1 7RH UK
[4]Neurobiology, Department Biology II, Ludwig-Maximilians-University Munich, Germany
[5] Autifony Srl laboratories, Medicines Research Centre, 37135 Verona, Italy.
[6] Department of Biomedical Sciences, College of Medicine, Florida State University, Tallahassee, FL 32306, USA

Corresponding author: Conny Kopp-Scheinpflug
Division of Neurobiology, Department Biology II,
Ludwig-Maximilians-University Munich,
Großhaderner Strasse 2, 82152, Planegg-Martinsried, Germany
voice: +49 (0) 89218074310, email: cks@bio.lmu.de

Running head: activity dependent size gradient
Figures: 6
Tables: 1
Abstract: 229 words
Introduction: 495 words
Discussion: 1619 words

Keywords: PMCA2, calyx of Held, synaptic transmission, auditory brainstem, tonotopic gradients

Acknowledgements: This research was funded by an Auditory Neuroscience Training Grant DC005361 (JHW), RO1 DC02739 (BLT), P30Core DC04661 (EWR), R01 DC03829 (EWR), DFG SFB870/2-A10 (CKS), MRC K005170 (IDF). We thank Brandon Warren for continuous support with the *in vivo* software and Linda Robinson for mouse care and genotyping.

Author contributions:

JHW: conducted anatomical measurements and jointly wrote manuscript

CKS: conducted *in vivo* recordings, capacitance measures *in vitro* and jointly wrote manuscript

NP: performed synaptic physiology *in vitro*

YW: helped with PMCA2 immunostaining

IDF: supervised *in vitro* electrophysiology and jointly wrote manuscript

EWR: provided material/advice on DTR mice and gerbil TTX experiments, provided advice on anatomical analyses and jointly wrote manuscript

BLT: conceived project, interpreted data and jointly wrote manuscript

Abstract

The medial nucleus of the trapezoid body (MNTB) is an important source of inhibition during the computation of sound location. It transmits fast and precisely timed action potentials at high frequencies; this requires an efficient calcium clearance mechanism, in which the plasma membrane calcium ATPase 2 (PMCA2) is a key component. Deafwaddler (*dfw*^{2J}) mutant mice have a null mutation in PMCA2 causing deafness in homozygotes (*dfw*^{2J}/*dfw*^{2J}) and high frequency hearing loss in heterozygotes (+/*dfw*^{2J}). Despite the deafness phenotype, no significant differences in MNTB volume or cell number were observed in *dfw*^{2J} homozygous mutants, suggesting PMCA2 is not required for MNTB neuron survival. The MNTB tonotopic axis encodes high to low sound frequencies across the medial to lateral dimension. We discovered a cell size gradient along this axis: lateral neuronal somata are significantly larger than medially located somata. This size gradient is decreased in +/*dfw*^{2J} and absent in *dfw*^{2J}/*dfw*^{2J}. The lack of acoustically driven input suggests that sound-evoked activity is required for maintenance of the cell size gradient. This hypothesis was corroborated by selective elimination of auditory hair cell activity using either hair cell elimination in Pou4f3 DTR mice or inner ear tetrodotoxin (TTX) treatment. The change in soma size was reversible and recovered within 7 days of TTX treatment, suggesting that regulation of the gradient is dependent on synaptic activity, and that these changes are plastic rather than permanent.

New and Noteworthy

Neurons of the medial nucleus of the trapezoid body (MNTB) act as fast-spiking inhibitory interneurons within the auditory brainstem. The MNTB is topographically organized with low sound frequencies encoded laterally and high frequencies medially. We discovered a cell size gradient along this axis: lateral neurons are larger than medial neurons. The absence of this gradient in deaf mice,

lacking the plasma membrane calcium ATPase 2 suggests an activity-dependent, calcium-mediated mechanism that controls neuronal soma size.

Introduction

Action potentials generated from both ears are transmitted to the superior olivary complex (SOC) via the globular and spherical bushy cells of the anterior ventral cochlear nucleus. Ipsilateral excitatory and contralateral inhibitory projections are integrated in the lateral superior olive (LSO) to calculate interaural intensity differences (IIDs; see Tollin 2003 for review). Although the excitatory input to the LSO is direct, the inhibitory circuit includes a signal inversion upon transmission through the medial nucleus of the trapezoid body (MNTB). These projections must converge in temporal register (Tollin 2003) and hence require fast transmission in the globular bushy cell–MNTB pathway to compensate for the additional synapse (Taschenberger and von Gersdorff 2000; Wang et al. 1998). MNTB neurons are driven by large glutamatergic synapses, the calyces of Held (Schneggenburger and Forsythe 2006; von Gersdorff and Borst 2002), and can sustain *in vivo* instantaneous firing rates of over 300 spikes per second (Kopp-Scheinpflug et al. 2008). With such high firing frequencies, presynaptic residual calcium must be cleared rapidly to avoid synaptic facilitation and/or depression. Similarly, calcium accumulation must also be controlled in the postsynaptic MNTB neuron.

PMCA2, the most efficient of the plasma membrane calcium ATPases, is localized in the stereocilia of sensory hair cells in the cochlea and is necessary for hair cell survival (Dumont et al. 2001; Kozel et al. 2002; Kozel et al. 1998; McCullough and Tempel 2004; Street et al. 1998; Takahashi and Kitamura 1999; Yamoah et al. 1998). Spontaneous mutations in the gene that encodes PMCA2 decrease expression and are associated with hearing loss both in humans and mice (Brini et al. 2007; Ficarella et al. 2007; McCullough et al. 2007; Schultz et al. 2005). These mutations in mice provide a valuable genetic tool to study PMCA2 in a mammalian model. The first PMCA2 mutant discovered was *deafwaddler* (*dfw*) which

results in a phenotype with auditory and vestibular deficits. The *dfw* point mutation renders the PMCA2 pump 60% less efficient compared to the wild type (Street et al. 1998; Penheiter et al. 2001). Another example is the dfw^{2J} mutation which is a frameshift mutation resulting in a premature stop codon (Street et al. 1998). Homozygous dfw^{2J} mutants (dfw^{2J}/dfw^{2J}) produce no PMCA2 protein, causing a more severe phenotype of deafness and ataxia, while heterozygous mutants ($+/dfw^{2J}$) exhibit a phenotype limited to high frequency hearing loss (McCullough et al. 2007). PMCA2 is highly expressed in avian brainstem neurons involved in sound localization and its expression is regulated by synaptic activity (Wang et al. 2009), but little is known about PMCA2 expression and function in the central auditory pathway of mammals.

Here we use anatomical, pharmacological and electrophysiological methods to study the expression and function of PMCA2 in the MNTB. We show that unlike in the peripheral auditory system, PMCA2 is not necessary for neuronal survival in the MNTB. Unexpectedly, we discovered a tonotopically organized cell size gradient in the MNTB that is regulated by sound-evoked activity and is absent in the deaf PMCA2 mutants.

Materials and Methods

Animals. Adult (5-7 weeks old) CBA/CaJ deafwaddler (dfw^{2J}), CBA/CaJ deafwaddler (*dfw*) (Street et al. 1998), and Pou4f3 DTR mice (Golub et al. 2012; Mahrt et al. 2013; Tong et al. 2015) of either sex were obtained from the University of Washington breeding colonies. Mice were genotyped using DNA obtained from tail biopsies. PCR amplification of the mutation (dfw) or insertion (DTR) were electrophoresed through an agarose gel and samples were detected using ethidium bromide and a transilluminator. For dfw^{2J} mutants, genotyping was done using a Taq-man SNP genotyping assay (Applied Biosciences). Detailed protocols are available online (http://depts.washington.edu/tempelab/Protocols/DFW2J.html). All manipulations were carried out in

accordance with protocols approved by the University of Washington Animal Care Committee and were performed in accordance with the NIH Guide for the Care and Use of Laboratory Animals.

Diphtheria toxin treatment. Diphtheria toxin (DT) was administered to diphtheria toxin receptor (DTR) mice, genetically engineered to express the human DTR selectively in hair cells (Tong et al. 2015). A single 25µg/kg dose of DT (List Biological Laboratories, Inc. #150) was delivered via intramuscular injection to four weeks old DTR mice. Within 6 days after DT injection, the DTR mice lose all of their hair cells and are completely deaf (Tong et al. 2015). After DT injection, DTR mice were allowed to survive for two weeks before tissue collection.

Histology. The animals were anesthetized with an overdose of Nembutal and perfused with a saline-heparin solution followed by 4% paraformaldahyde. The brains were exposed in the skull and stored in 4% paraformaldahyde overnight. The brains were then dissected from the skull and post-fixed for an additional hour. The tissue was transferred to 10% sucrose in 0.1M phosphate buffer until sinking which took approximately 3 hours. The tissue was transferred again to 30% sucrose in 0.1M phosphate buffer where they remained until sinking, which took approximately 24 hours. Coronal sections of 10 or 40 µm thick were cut through the brain stem using a cryostat or freezing stage on a sledge microtome. Free floating sections were stored in phosphate-buffered saline (PBS; pH 7.4).

Immunocytochemistry. The fixed sections were treated with primary antibody for PMCA2 (dilution 1:250) in PBS with 0.3% Triton X-100 for 2 hours at room temperature and washed in PBS overnight at 4°C. The sections were then incubated with microtubule associated protein 2 (MAP2) primary antibody at 1:1000 in PBS with 0.3% Triton X-100 for 1.5 hours at room temperature. The sections were washed in PBS before incubating in AlexaFluor secondary antibodies (1:200; Molecular Probes, Eugene, OR) for 2 hours at room temperature. The sections were treated with DAPI before coverslipped with Fluoromount-G (Southern Biotech).

Primary Antibodies. Polyclonal anti-PMCA2 (catalog No. PA1-915, rabbit) was purchased from Affinity Bioreagents (Golden, CO). The immunogen was a synthetic peptide corresponding to amino acid residues 5-19 of human PMCA2 protein, sequence: TNSDFYSKNQRNESS. This sequence is conserved between human and mouse PMCA2. Monoclonal anti-MAP2 (catalog No. MAB3418, mouse) was purchased from Chemicon International. The immunogen was bovine brain microtubule protein and binds to MAP2a and MAP2b.

Nissl Staining. Alternate sections from each animal were mounted and stained with thionine for 5 minutes and then dehydrated in xylene, mounted and coverslipped with DPX (SIGMA).

Confocal Microscopy. Images for the ICC experiment were taken with an Olympus FV-1000 Confocal microscope using an oil 100x objective. A 5.6 µm thick z-stack was deconvolved using the Huygens deconvolution system. The image was cropped to contain one cell (approximately ¼ of the original image). Brightness and contrast were adjusted to maximize visualization of the calyx.

Light Microscopy. Images for morphology experiments were taken with a Zeiss Axioplan 2ie using a 10x or 40x objective. Each section was positioned so that the midline was perpendicular or parallel to the x-axis of the image. The focal plane selected for these images was approximately in the center of the section thickness to the nearest micron. For 10x magnification one image was taken. For 40x magnification 1-16 images were taken covering the entirety of the MNTB in that section. The 40x images were used to generate a montage using MosaicJ in ImageJ and saved as one image.

Profile counts. To determine the number of neurons in each MNTB, all neurons in the MNTB of stained sections were counted online using a counting grid. The slides were randomized to blind the counter to the genotype of the tissue. The experimenter focused up and down with a 40x objective in each square of a counting grid. Only neurons with a nucleus and nucleolus were counted. The total number of neurons present in each MNTB was estimated by multiplying by 2 since only half of the slices were analyzed (Figure 2A).

163 *MNTB Volume.* The volume of the nucleus was determined using the cross sectional area of the
164 MNTB in each thionine stained section. Images of the MNTB in each section were taken using a 10x lens
165 and randomized for blind analysis. The MNTB was outlined using ImageJ, only cells that were darkly
166 stained and less than 20μm from their nearest neighbor were included in the MNTB perimeter. This
167 outline was used to calculate the area of the MNTB in each section. The volume of the MNTB was
168 estimated by multiplying each MNTB area by 40μm. This value was doubled since only every other
169 section of the MNTB was analyzed. These individual areas were summed to find the total volume of
170 each MNTB (Figure 2B).
171 *Neuron Size.* Neuron size was measured using 40x montaged images of coronal sections such that the
172 montage included the entire extent of the nucleus in any given section. Each montaged image was given
173 a random number file name to blind the experimenter to genotype and subject identity. All cells in the
174 montaged image that contained a defined nucleus, nucleolus, and unobstructed cell membrane were
175 analyzed. The cross sectional area of the neuron as well as the x and y coordinates of the region of
176 interest's central pixel within the image were obtained using the algorithm provided by ImageJ (Figure
177 2C). The x and y coordinates were then used to calculate the distance from the midline of the brain
178 section for each individual neuron.
179 *Tonotopic Axis.* The tonotopic gradient in the MNTB extends from neurons encoding high
180 frequencies dorsomedially to neurons encoding low frequencies ventrolaterally (Sonntag et al. 2009).
181 Therefore the tonotopic axis was defined as the longest dorsomedial to ventrolateral line that could be
182 drawn through the MNTB to estimate the expected tonotopic axis in each montaged image of the
183 coronal sections. This line was divided into thirds; and then two additional lines were drawn
184 perpendicular to the tonotopic axis to delineate medial, central and lateral areas.
185 *Slice preparations.* Mice (P13–P20) were killed by decapitation in accordance with the UK Animals
186 (Scientific Procedures) Act 1986 and brainstem slices containing the superior olivary complex (SOC)

prepared as previously described (Tong et al. 2013). Transverse slices (200 µm-thick) containing the MNTB were cut in a low-sodium artificial CSF (aCSF) at ~0°C. Slices were maintained in a normal aCSF at 37°C for 1 hour, after which they were stored at room temperature (~20°C) in a continually recycling slice-maintenance chamber. Composition of the normal aCSF was (mM): NaCl 125, KCl 2.5, $NaHCO_3$ 26, glucose 10, NaH_2PO_4 1.25, sodium pyruvate 2, myo-inositol 3, $CaCl_2$ 2, $MgCl_2$ 1 and ascorbic acid 0.5; pH was 7.4, bubbled with 95% O_2, 5% CO_2. For the low-sodium aCSF, NaCl was replaced by 250 mM sucrose, and $CaCl_2$ and $MgCl_2$ concentrations were changed to 0.1 and 4 mM, respectively. Experiments were conducted at a temperature of 36^{o}C±1 using a Peltier driven environmental chamber (constructed by University of Leicester Mechanical and Electronic Joint Workshops) or using a CI7800 (Campden Instruments, UK) feedback temperature controller.

Patch-clamp recording. Whole-cell patch-clamp recordings were made from visually identified MNTB neurons (40X water-immersion objective, differential interference contrast optics) using an Axopatch 200B amplifier/Digidata 1440 (synaptic physiology) or a Multiclamp 700B amplifier (capacitance measures) and pClamp-10 software (Molecular Devices, Sunnyvale, CA, USA), sampling at 50kHz and filtering at 10kHz. Patch pipettes were pulled from borosilicate glass capillaries (GC150F-7.5, OD: 1.5mm; Harvard Apparatus, Edenbridge, UK) using a two-stage vertical puller (PC-10 Narishige, Tokyo, Japan). Their resistance was ~3.0 MΩ when filled with a patch solution containing (mM): KGluconate 97.5, KCl 32.5, HEPES 40, EGTA 5, $MgCl_2$ 1, Na_2phosphocreatine 5, pH was adjusted to 7.2 with KOH. Osmolarity was around 300 mOsm. Voltage signals were not corrected for the liquid junction potential (-11 mV). Whole-cell series resistances were <10MΩ, compensated by 70% and recordings in which the series resistance changed more than 2MΩ were eliminated from analysis. EPSCs were elicited by stimulation through a bipolar platinum electrode positioned across the midline. The stimulating electrode was connected to a voltage stimulator (DS2A, Digitimer Ltd, UK) delivering 200 µs, 5-50V pulses at a rate of 0.25 Hz. The voltage-stimulus was adjusted to give a large synaptic response from one calyceal input in

each recording. EPSCs were recorded in the presence of 10µM bicuculline, 0.5-1µM strychnine, and 50µM D-AP5. Tetrodotoxin (TTX, 0.5µM) was added in addition to the above cocktail to record mEPSCs. All chemicals and drugs were obtained from Sigma (UK) with the exception of: bicuculline, 2-amino-5-phosphono-pentanoic acid (D-AP5) from Tocris (Bristol, UK). EPSC decay times and amplitudes were measured from averaged traces (10-15 records). mEPSC decay times were measured from averaged traces (20 records). The holding potential was set to -40mV.

Capacitance measures. Cell capacitance was assessed in whole-cell voltage-clamp recordings using the pCLAMP-10 software. For each neuron the capacitance value was read out directly as the telegraphed signal from the amplifier. At the end of each recording, a low magnification (4x) image was taken to document the location of the pipette tip (still in the cell) with respect to the midline. These images were then used to divide the MNTB into a medial, central and lateral division as introduced above.

In vivo recordings. Spontaneous and sound-evoked MNTB neuron responses were recorded from 16 adult mice (3 dfw^{2J}/dfw^{2J}; 13 wild type CBA/Ca). During surgical preparation and recording, animals were anesthetized by intraperitoneal injection of a mixture of ketamine hydrochloride (100mg/kg BW) and xylazine hydrochloride (5mg/kg BW). The level of anesthesia was maintained by hourly subcutaneous injections of one-third of the initial dose. MNTB single unit recordings characteristically possess a prepotential, followed by a biphasic postsynaptic action potential and, in the wild type, responded to sound from the contralateral ear (Kopp-Scheinpflug et al. 2003). The characteristic waveform allowed identification of spontaneous MNTB neuron firing even in the deaf mice. Spontaneous firing was recorded for a period of 4 seconds. Synaptic delay was measured from peak to peak between the prepotential and the postsynaptic action potential (Fig. 1G).

TTX Experiments. All measurements for the TTX experiments were carried out using tissue previously collected by Pasic and Rubel (Pasic et al. 1994; Pasic and Rubel 1991). These studies used adult

Mongolian Gerbils of either sex. Cochlear ablations were performed by removing the pinna, incising the tympanic membrane of one ear, and removing the malleus. The bony walls of all three turns of the cochlea were then opened, the cochlear contents were crushed and aspirated, and the modiolus was fractured. For TTX treatment, TTX crystals (Sigma Chemicals, St. Louis, MO) were suspended and placed on a disk of ethylene-vinyl acetate copolymerresin (Elvax). Small pieces of the disk (0.1g) containing approximately 500ng of TTX were cut with a 17-gauge stub adapter. TTX blockade of eighth nerve activity was obtained by making an incision posterior to the ear canal, opening the mastoid bulla, and placing the disk with TTX in the round window niche of the middle ear, resting against the round window membrane. In animals receiving TTX treatment for 48 hours, the TTX disc was replaced after 24 hours to ensure adequate maintenance of the block. Animals in the group which survived for 7 days had the disk containing TTX removed 20 or 44 hours after insertion. Previous experiments showed that soma size of neurons in the cochlear nucleus are unaffected by placing polymer without TTX in the round window (Pasic and Rubel 1989) and that blockade reliably lasted for 4 hours following removal of the disc (Pasic and Rubel 1991). All treatment was unilateral and the MNTB contralateral to the treated ear was used for analysis. See Pasic and Rubel (1991; 1989) for complete methods.

Data analysis and statistical methods. Statistical analyses of the data were performed with SigmaStat/SigmaPlot™ (SPSS Science, Chicago, IL) or Prism (GraphPad, La Jolla, CA). Results are reported as mean ± s.e.m; n = the number of animals for histological data and the number of neurons recorded from at least 3 different animals for electrophysiology data. Statistical comparisons between different data sets were made using unpaired Student's *t*-test or ANOVA. Differences were considered statistically significant at $p<0.05$.

Results

PMCA2 is involved in the regulation of presynaptic transmitter release at the calyx of Held

Immunocytochemical experiments demonstrated that PMCA2 is expressed throughout the MNTB. High resolution images showing cross-sections through a single MNTB neuron and the calyx of Held, show that PMCA2 is present both presynaptically and postsynaptically (Figure 1 A-B). The cross section through the calyx shows the inner and outer membrane (arrows) of the calyx. PMCA2 is clearly present in the calyx, indicating it is involved in presynaptic calcium clearance. PMCA2 is also present in the soma of post-synaptic neurons where it is likely to be involved in postsynaptic calcium clearance or to be transported into the downstream synapses.

A presynaptic rather than postsynaptic action of PMCA2 was supported by the analysis of miniature excitatory postsynaptic currents (mEPSCs) during *in vitro* whole cell patch clamp recordings. The lack of presynaptic PMCA2 in the dfw^{2J}/dfw^{2J} mice caused an increase in mEPSC frequency from 16.6 ±6.0 Hz (n=4) in the wild type to 38.1 ±4.6 Hz (n=4; p=0.029) in the dfw^{2J}/dfw^{2J} suggesting a presynaptic increase in transmitter release (Figure 1C). The amplitude of the mEPSCs remained unaltered (WT: 55.3 ±10.2pA; dfw^{2J}/dfw^{2J}: 50.8 ±13.8 pA; p=0.791). Activation of the calyx of Held input via electric fiber stimulation at the midline showed an increase in AMPAR conductance from 132.7 ±16.0 nS (n=18) in the wild type to 187.9 ±14.5 nS (n=17; p=0.015) in the dfw^{2J}/dfw^{2J}, while decay time constants were unchanged between genotypes (Figure 1D). Extracellular recordings of single MNTB neurons *in vivo* in the dfw^{2J}/dfw^{2J} mice revealed no sound-evoked activity while stimulating the contralateral ear with either pure tones or noise pulses up to 90 dB SPL (data not shown). However, the *in vivo* recordings allowed the acquisition of spontaneous firing rates which were significantly increased in the dfw^{2J}/dfw^{2J} mice (81.9 ±21.70 Hz; n=13) compared to their wild type controls (25.7 ±4.0 Hz; n=65; p=0.001; Figure 1E). The large somatic calyx synapses that innervate each MNTB neuron give rise to a typical complex waveform from *in vivo* extracellular recordings (Guinan and Li 1990; Kopp-Scheinpflug et al. 2003) consisting of a presynaptic potential (prepotential) and a postsynaptic action potential (recording traces in Fig. 1F). The prepotential and the postsynaptic action potential are separated by a synaptic delay which was shorter

in the *dfw*^{2J}/*dfw*^{2J} mice (0.38 ±0.01ms; n=13) compared to the wildtypes (wt: 0.47 ±0.02ms; n=14; *p*=0.002; Figure 1F).

Figure 1 (double column) about here

Together these data support the hypothesis that PMCA2 is involved in the regulation of presynaptic transmitter release at the calyx of Held. To test if PMCA2 is necessary for neuronal survival or normal neuronal morphology, the MNTB neuron number (Figure 2A), nucleus volume (Figure 2B) and neuron size (Figure 2C) were measured in Nissl stained sections from +/+ littermates, +/*dfw*^{2J}, and *dfw*^{2J}/*dfw*^{2J} mice. Each MNTB contained on average 2551 (wild type), 2436 (+/*dfw*^{2J}) and 2563 (*dfw*^{2J}/*dfw*^{2J}) neurons. Average MNTB volumes were 42.25µm^3, 43.17 µm^3, 35.46 µm^3 and 39.07 µm^3 in wild types, +/*dfw*^{2J}, dfw/dfw and *dfw*^{2J}/*dfw*^{2J} mice respectively. Statistical analysis confirmed that there was no significant difference in neuron number (Figure 2A, D; F=0.1310; *p*=0.8797) or in the volume of the MNTB nucleus (Figure 2B,E; F=1.965; *p*=0.4508) between the genotypes.

Figure 2 (double column) about here

A cell size gradient discovered in wild type mice is absent in PMCA2 mutants (*deafwaddler mice)*

MNTB neurons were significantly smaller in *dfw*^{2J}/*dfw*^{2J} (128.36 µm^2 ±7.54) than in wild type (151.89 µm^2±1.11; Figure 2C,F; F=5.894; *p*=0.04). To determine if these differences showed any tonotopic relationship, the nucleus was divided into thirds and neurons were assigned to medial, central, or lateral groups (Figure 3A). We defined PMCA2 function as the percentage of PMCA2 protein, determined by the number of functional alleles possessed by an animal, multiplied by the PMCA2 pumping efficiency, determined by biochemical assay (Penheiter et al., 2001) and compared to wild type. We tested a range of PMCA2 function from wild type (which have 100% protein), +/*dfw*^{2J} with about 50% protein, *dfw*/*dfw* with approximately 30% function as measured by a calcium clearance assay (Penheiter et al. 2001), and *dfw*^{2J}/*dfw*^{2J} which have no functional PCMA2 protein (Table 1). In wild type animals, medial neurons were significantly smaller (136.01 µm^2 ±2.66) than lateral neurons (157.71 µm^2±5.05; Figure 3B; *p*=0.02).

In +/*dfw*^{2J}, the location-dependent difference in neuronal cell size was decreased and no longer significant (Figure 3B; *p*=0.08). In *dfw*/*dfw* the size difference was decreased further and was absent in the *dfw*^{2J}/*dfw*^{2J} mice (Figure 3B). Although absolute neuronal soma size varied slightly between animals, comparing the size difference in medial and lateral neurons for each individual mouse confirmed the presence or absence of the overall size gradient in the different genotypes (Figure 3C). Neuronal soma size data of all measured individual neurons from one wild type MNTB and one *dfw*^{2J}/*dfw*^{2J} MNTB are shown as an example in Figure 3D. The slope of the linear regression for neuronal soma size is significantly non-zero in wild type mice (Figure 3D; *p*=0.01) while no relationship between neuronal soma size and tonotopic location was found in *dfw*^{2J}/*dfw*^{2J} demonstrating that there is a neuronal cell size gradient in wild type which is absent in *dfw*^{2J}/*dfw*^{2J}.

Figure 3 (single column) about here

A medial to lateral increase in membrane capacitance is accompanied by larger synaptic input in wild type but not in *dfw*^{2J} mutants

As a complementary measure of neuronal soma size, somatic surface area was assessed by determining the cell membrane capacitance C_m in voltage-clamp recordings of MNTB neurons and comparing it across the tonotopic axis (see methods). In wild type mice, medial MNTB neurons had a smaller (C_m: 9.75 ±2.47 pF; n=28) capacitance than lateral MNTB neurons (C_m: 13.75 ±0.72 pF; n=28; Fig. 4B, *p*=0.001), corroborating the size gradient measured in the histological experiments. The difference in cell membrane capacitance between medial and lateral neurons was completely abolished in +/*dfw*^{2} mice (medial C_m: 11.87 ±0.55 pF; n=14; lateral: C_m: 12.72 ±1.03 pF; n=9; *p*=0.463) as well as in *dfw*^{2J}/*dfw*^{2J} mice (medial C_m: 11.14 ±0.54 pF; n=16 vs. lateral C_m: 11.79 ±0.42 pF; n=16; *p*=0.344). When compared across genotypes the differences in capacitance between medial neurons or lateral neurons were not significantly different (RM ANOVA). No systematic changes in input resistance between medially and laterally patched cells in the MNTB of wild type, +/*dfw*^{2J} or *dfw*^{2J}/*dfw*^{2J} mice were observed (RM ANOVA:

331 p=0.257). In contrast, membrane time constants (τ) in wild type MNTB were significantly faster in medial
332 (7.4 ±0.7ms; n=16) than in lateral neurons (10.8 ±1.0ms; n=16; p=0.007) while no such correlation was
333 found in the +/dfw^{2J} or dfw^{2J}/dfw^{2J} mice (data not shown).

334 The difference in soma size between medial and lateral MNTB neurons raised the question of
335 whether the synaptic current or the neuronal output firing also varied across the tontopic axis? Our
336 initial experiments (Fig. 1) comparing overall EPSCs between wild type and dfw^{2J}/dfw^{2J} mice already
337 showed larger EPSCs in the dfw^{2J}/dfw^{2J} mice. Sorting the EPSCs according to the location of the neurons
338 within the MNTB revealed significantly larger EPSCs in lateral, low-frequency MNTB neurons (8.4 ±0.4
339 nA; n=3) than in the medial, high-frequency neurons (4.2 ±0.7 nA; n=7; p=0.007; Figure 4C). In the
340 dfw^{2J}/dfw^{2J} mice calyceal inputs to medial and lateral neurons were equally large (med: 7.7 ±0.7 nA; n=7;
341 lat: 7.5 ±1.3 nA; n=6; p=0.931). Larger EPSCs in lateral, low-frequency MNTB neurons could affect either
342 firing rates or temporal precision or both. *In vivo* recordings in wild type MNTB neurons showed no
343 significant correlation of characteristic frequency (i.e. location along the medial-to-lateral axis) with
344 either spontaneous (Pearson correlation: p=0.53) or maximum firing rates (Pearson correlation: p=0.73;
345 Fig. 4D). In contrast, a significant correlation (Pearson correlation: p=0.008) between the coefficient of
346 variation (CV) of the first spike latency (FSL) to sound-evoked responses and the characteristic frequency
347 was found in wild type mice (Figure 4D). The deafness phenotype of the dfw^{2J}/dfw^{2J} mice did not allow a
348 similar analysis in the mutant.

349 **Figure 4 (single column) about here**

350 **The lack of auditory activity reversibly eliminates the neuronal cell size gradient in the MNTB**

351 *In vivo* recordings of MNTB neurons revealed that the dfw^{2J}/dfw^{2J} mice have no measurable
352 responses to sound but maintained spontaneous action potential firing activity (Figure 1F) which is
353 known to be generated in and propagated from the cochlea (Lippe 1994; Tritsch et al. 2010). To
354 determine if the elimination of cochlear activity could also cause a change in the neuronal cell size

gradient, we used three different approaches (Table 1): First, we eliminated all cochlear hair cells by administering diphtheria toxin (DT) to mice which selectively express the human diphtheria toxin receptor (DTR) in their hair cells (Tong et al., 2015). These mice showed an overall decrease in MNTB neuronal cell size by about 30% compared to the wild type and no significant difference in size between medial and lateral neurons (Figure 3B, C). Second, we used tissue from animals either 24 or 48 hours after cochlear ablation. These experiments were performed in gerbils which are slightly larger than mice; this simplifies the surgery and at the same time allows a generalization of the activity-dependent neuronal cell size gradient to a mammal that hears in the lower frequency range. Similar to the data from wild type mice we found that medial neurons (151.26 ±2.03 μm^2) in the gerbil MNTB are significantly smaller than lateral neurons (177.51 ±3.32 μm^2; Figure 5; $p \leq 0.001$). Twenty four hours after cochlear ablation, the difference in size between medial and lateral neurons was still significant (Figure 5A; $p=0.01$), but 48 hours after cochlear ablation, the difference was no longer significant, indicating that the size gradient had decayed (Figure 5). The third approach to eliminate cochlear activity asked if the loss of the neuronal soma size gradient following sensory deprivation was reversible. The sodium channel blocker tetrodotoxin (TTX), which prevents the generation of action potentials in the spiral ganglion cells and therefore eliminates all cochlear driven activity, was applied via the round window (see methods). After 24 hours of TTX treatment, the size difference between medial and lateral neurons was no longer significant and by 48 hours, the soma size was indistinguishable between medial and lateral cells (Figure 5). Data for the average sizes for medial, central, and lateral neurons are shown for each individual gerbil (Figure 5B).

The pharmacological blockade of sodium channels by TTX was reversible, so that after TTX was removed, the cochlea recovers and activity resumes. In animals that were allowed to recover for 7 days from a 48 hour TTX treatment, the size gradient was restored and lateral neurons were again larger than medial neurons (Figure 5; $p=0.02$).

Figure 5 (single column) about here

Discussion

The results of this study show a medial to lateral cell size gradient in the MNTB. This gradient is dependent on afferent activity and can be reversibly abolished when the input activity is lost. While TTX and DT treatment or cochlear ablation completely eliminate all input activity, the deafwaddler mutation maintains spontaneous firing but cannot transmit additional sound-evoked activity. All of these manipulations led to smaller cells. If there was a simple or linear correlation between firing rate and cell size, then we would have predicted a uniformly large cell size in the *dfw*^{2J} mutants, given the high spontaneous firing rates of the mutant mice. However, general afferent activity (spontaneous firing) alone did not lead to larger lateral neurons. Therefore our observations suggest a more complex control of soma size, perhaps including the release of calcium-dependent signals controlling the size of the lateral neurons. Sound-frequency specific input characteristics seem necessary to induce and maintain the neuronal size gradient and PMCA2 is involved in regulating these inputs.

Figure 6 (single column) about here

Tonotopic gradients in the auditory system

Tonotopic organization is first established in the cochlea where the location of hair cells along the basilar membrane dictates the characteristic frequency to which the hair cells respond through both physical resonance and molecular signaling mechanisms. This organization is propagated to many higher levels of the auditory brainstem and all the way to the auditory cortex. Tonotopic gradients in cell morphology and size as well as gradients involving ion channels and receptors are well established for many different parts of the auditory pathway: The hair cells in the cochlea show differences in stereocilia length and somata size. Apical cells, responding best to low frequencies, have longer

403 stereocilia and larger somata; while basal cells, responding to high sound frequencies, have shorter
404 stereocilia and smaller somata (Ashmore and Gale 2000; Corwin and Warchol 1991; Tilney et al. 1987).
405 For example, in the spiral ganglia there is a tonotopic arrangement of synaptic proteins associated with
406 greater expression of α-GluR2/3 in high-frequency neurons than in low-frequency neurons (Flores-Otero
407 and Davis 2011). In the MNTB ion channel gradients of Kv3 decreases across the medial to lateral
408 tonotopic axis (Leao et al. 2006; von Hehn et al. 2004) while an inverse Kv1 gradient increases from
409 medial to lateral MNTB (Gazula et al. 2010; Leao et al. 2006). These tonotopic gradients have been
410 recognized throughout the developing and mature auditory pathways (Rubel 1978; Smith and Rubel
411 1979) and are considered essential features for each neuron to optimally perform specialized tasks
412 (within the context of achieving temporal precision and information transmission across a range of
413 firing). In this study we have characterized a cell size gradient in the MNTB which is dependent on
414 auditory activity. As summarized in Figure 6, four independent approaches were employed to test if
415 maintenance of the gradient requires active auditory inputs. Two methods utilized mouse transgenic
416 mutants and two used surgical and pharmacological manipulation of the cochlea in gerbils. The TTX
417 treatment in gerbils provided a reversible procedure which demonstrated that the neuronal size
418 gradient in the MNTB is able to recover after a period of sensory deprivation. A previous publication
419 noted a difference in MNTB cell size between medial and lateral cells (Pasic and Rubel 1991). However
420 at that time we were unable to relate a continuous gradient to the tonotopic organization of MNTB.
421 Previous reports have eliminated all cochlea driven activity (both sound-evoked and spontaneous); but
422 the dfw^{2J}/dfw^{2J} model used in the present study allowed distinction between the influence of
423 spontaneous versus sound-evoked activity. Mutant dfw^{2J}/dfw^{2J} mice are deaf (Street et al. 1998) and no
424 acoustically driven activity could be recorded in the MNTB of these mice. However, high levels of
425 spontaneous activity are maintained and were recorded in the MNTB of dfw^{2J}/dfw^{2J} mice. Further

426 investigations will be required to determine if the size gradient develops if either high or low frequency
427 input is eliminated before hearing onset.
428
429 **How PMCA2 could affect gradients of MNTB function along the medial-to-lateral axis**
430 Knowledge of PMCA2 expression along the medial-to-lateral axis in the MNTB would provide insight into
431 how PMCA2 could influence MNTB function. However, immunohistochemical labeling is difficult to
432 quantify and the MNTB is too small to provide sufficient protein for Western blot analysis of medial and
433 lateral divisions, especially given that this method could also not distinguish between calyceal and
434 somatic PMCA2. Therefore in the present study we used physiological parameters to test postulates
435 concerning PMCA2 expression within the MNTB. Lateral neurons of wild type animals have larger EPSC
436 amplitudes which *in vivo* can cause either a higher MNTB firing rate or higher temporal precision, or
437 both. We plotted the *in vivo* firing rates against the tonotopic (medial-to-lateral) axis and found no
438 significant correlation. In contrast, plotting the coefficient of variation of the first spike latency (as a
439 measure of temporal precision) against the tonotopic axis showed low CVs in the low frequency (lateral)
440 MNTB neurons. Unfortunately the deafness phenotype of the dfw^{2J}/dfw^{2J} mice did not allow a similar
441 analysis in the mutant, but the wild type data corroborate the idea that low frequency (lateral) calyx
442 synapses express less PMCA2 which results in less suppression, larger EPSCs and well timed action
443 potentials in the low frequency neurons. Rather than arguing for an "increased" EPSC amplitude in
444 medial MNTB of dfw^{2J} mice, we interpret this result as less suppression of the EPSCs, compared to their
445 wild type counterparts. The amplitude of the synaptic response strongly depends on basal and dynamic
446 presynaptic calcium concentrations in the terminal (Billups and Forsythe 2002; Bollmann et al. 2000;
447 Kochubey et al. 2009). PMCA2 in the wild type calyx of Held contributes to calcium clearance from the
448 terminal, while in the dfw^{2J} mutant the lack of PMCA2 in the calyx of Held slows calcium extrusion rates
449 and raises basal intracellular calcium concentrations, creating a complex interaction with multiple

mechanisms of short-term plasticity (Muller et al. 2010) and causing increased transmitter release. Applying similar logic to the differences in EPSC size between medial and lateral MNTB neurons in the wild type, leads to the conclusion that PMCA2 is more highly expressed in the medial MNTB and this causes the smaller EPSC amplitudes in medial neurons. Such a distribution of PMCA2 *in vivo* causes larger EPSCs with shorter synaptic delay and less timing jitter in lateral neurons. Higher PMCA2 expression in medial neurons would increase calcium clearance, causing EPSCs with chronically depressed amplitudes, which are sensitive to recent history but poorly timed (Lorteije et al. 2009).

The lack of PMCA2 in both the medial and the lateral MNTB neurons in the dfw^{2J} could be interpreted as medial dfw^{2J} neurons lacking the chronic depression present in wild type (so generating larger EPSC amplitudes in the mutant). Though it is not our intention to exclude a peripheral component to the net changes in auditory processing induced by the loss of the PCMA2, the larger amplitude of the calyx of Held EPSC in the mutant mice strongly supports a local and central mechanism of action, since each EPSC is generated by the action of a single synaptic input (the calyx) which has arisen from the globular bushy cell in the aVCN. Similar effects (increased EPSCs) in the periphery (at the hair cell or endbulb) might increase the frequency of action potential firing in the bushy cell axons, but would not directly influence the amplitude of evoked synaptic currents at the calyx. This interpretation is consistent with previous reports that the deafness phenotype of the *dfw* mutant arises in the cochlear hair cells as initially described (Street et al. 1998), while we conclude that the central expression of PMCA2 further affects transmitter release and neuronal cell size in the auditory brainstem (see paragraph below).

Balance between input size and cell size

The EPSC frequency and size are influenced by the available calcium in the presysnaptic terminal. Eliminating PMCA2 from the calyx of Held terminal will rraise presynaptic calcium concentrations, increasing transmitter release and causing larger EPSCs; whereas in wild type MNTB, PMCA2 will

maintain lower basal intracellular calcium concentrations, and thereby fine-tune synaptic strength (Billups and Forsythe 2002; Borst et al. 1995; Felmy and Schneggenburger 2004; Felmy and von Gersdorff 2006).

Membrane capacitance (C_m) is proportional to the surface area of a cell, and higher capacitance slows the neuronal membrane time constant: $\tau = R_m * C_m$ (where τ is the time constant and R_m is the resistance of the membrane) so that smaller neurons will fire more rapidly than large neurons (Franzen et al. 2015). The soma size gradient in the MNTB implies that medial cells (which are smaller than lateral cells) will fire more rapidly than the lateral cells. However, there are other demands on neurons; for example, one reason for larger cell bodies in the lateral, low frequency region of the MNTB might be a higher metabolic rate in these neurons. High metabolic rate is often associated with larger cells and it has been suggested that neurons which process signals with a high temporal resolution have especially high metabolic demands (Attwell and Laughlin 2001). The present results suggest the possibility of a homeostatic adjustment where larger synaptic inputs, which enable high temporal precision of the lateral MNTB neurons, are complemented by larger postsynaptic cells, and suggestive of higher metabolic demand.

Consequently, not only the cell size, but also increasing the rate or amplitude of the synaptic inputs increases the energy demands of the cell (Sengupta et al. 2013). We conclude that PMCA2 expression in these giant synapses innervating medial MNTB neurons causes synaptic suppression (compared to their lateral counterparts). This might reduce the energy demand of the medial neurons and trigger a reduction in neuronal size. Further work will be necessary to test these hypotheses.

Legends

Figure 1. PMCA2 regulates transmitter release in the MNTB. (A) Immunohistochemical labeling for MAP2 and PMCA2 in the MNTB and **(B)** in an individual MNTB neuron **(B)**. A cross section through the calyx is marked 'calyx'. Arrows show where PMCA2 appears to be localized presynaptically in the outer membrane of the calyx. (Red=PMCA2, Green=MAP2, Blue=DAPI). **C)** Voltage-clamp recordings from postsynaptic MNTB neurons in acute brain slices show a higher frequency of miniature excitatory postsynaptic currents (mEPSCs) in the MNTB of dfw^{2J}/dfw^{2J} mice (red) compared to wild type (black). **D)** Calyceal EPSCs evoked by midline stimulation are larger in dfw^{2J}/dfw^{2J} mice (red) compared to wild type (black). Stimulus artifacts have been deleted for clarity. WT data include 7 medial cells, 3 lateral cells and 8 cells with no information about location in the MTNB. Dfw^{2J}/dfw^{2J} data include 7 medial cells, 6 lateral cells and 4 cells with no information about location in the MTNB (see also Fig. 4C). **E, F)** *In vivo* single unit recordings of MNTB neurons measured **E)** higher spontaneous firing rates and **F)** shorter synaptic delays in dfw^{2J}/dfw^{2J} mice (red) compared to wild type (black).

Figure 2. MNTB Morphology is similar in wildtype and dfw^{2J} mutants. Nissl stained coronal sections were used to estimate **A)** cell number, **B)** MNTB volume, and **C)** average cell size in wild type, +/*dfw2J*, and dfw^{2J}/dfw^{2J} mutants. **D)** There was no significant difference in cell number between any of the genotypes (n=3 mice per group). **E)** There was no significant difference in MNTB volume between any of the genotypes (n=6 MNTB per group). **F)** There was a significant decrease in the average cross sectional area between wild type and dfw^{2J}/dfw^{2J} mutants (*$p \leq 0.05$, n=1854 cells from 9 mice). Error bars=s.e.m.

Figure 3. Medial to lateral soma size gradient in the MNTB is absent in the dfw^{2J} mutants. A) Cells were defined as medial if located in the medial third of the MNTB or lateral if located in the lateral third of the MNTB. **B)** There was a significant increase in the size of lateral cells as compared to medial cells in the wild type animals ($p \leq 0.001$). There was no significant increase in the size of lateral cells in the $+/dfw^{2J}$, *dfw/dfw,* dfw^{2J}/dfw^{2J}, or DTR mice. Error bars are s.e.m. **C)** Individual average cell size for medial

and lateral cells in each MNTB. **D)** Scatter plot of location along the tonotopic axis vs. cross sectional surface area for one MNTB from a wild type and *dfw*^{2J}/*dfw*^{2J}. The linear regression is significantly different from zero for wild type (p=0.01) but not for *dfw*^{2J}/*dfw*^{2J}.

Figure 4. Lateral MNTB neurons have a larger membrane capacitance and larger calyceal inputs in wild type but not in *dfw*^{2J} mutants. A) Cell membrane capacitance was acquired for visually identified neurons in voltage-clamp mode. Dye labeling of each neuron via the patch pipette allowed offline measurements of the neurons position within the MNTB. **B)** Capacitance measurements corroborate histology data showing lateral cells are significantly larger than medial cells in wild type (p≤0.001) but there is no significant difference between cells in +/*dfw*^{2} and *dfw*^{2J}/*dfw*^{2J} mutants. Error bars are s.e.m. **C)** Calyceal EPSCs are larger in lateral than in medial MNTB wild type neurons. No significant difference was found between EPSC amplitudes of medial and lateral neurons in *dfw*^{2J}/*dfw*^{2J} mutants. **D)** In *in vivo* recordings of single MNTB neurons in wild types, characteristic frequency is used as a measure for medial-to-lateral position. No significant correlation was found between medial-to-lateral position and firing rate. **E)** The coefficient of variation for the first spike latency (FSL) showed a positive correlation with characteristic frequency. Unfortunately, due to the deafness phenotype these data could not be acquired in the *dfw*^{2J}/*dfw*^{2J} mutants.

Figure 5. Lack of sensory input reversibly abolishes the soma size gradient in gerbils. A) Control gerbils showed a cell size gradient as did subjects with tissue collected 24 hours after cochlear ablation (p≤0.001 and p=0.01 respectively). Tissue collected 48 hours after cochlear ablation showed a diminished gradient. Gerbils treated with TTX for 24 or 48 hours showed a decreased or no cell size gradient, but in those animals allowed to recover for 7 days, the gradient had returned (p=0.02). Error bars are s.e.m. **B)** Individual average cell size for medial, central and lateral regions of each MNTB.

Figure 6. Sound-evoked auditory activity is required to maintain the soma size gradient in the MNTB of mice and gerbils. Normal hearing gerbils and mice both show a soma size gradient. If auditory

activity is eliminated through cochlear ablation (gerbil), or TTX treatment (gerbil), DT treatment (mouse) or genetic mutation (mouse) the cell size gradient is absent. If auditory activity returns after a period of deprivation (TTX treatment) the cell size gradient will be restored. Note, the dotted outline of the presumptive PMCA2 gradient indicates expression in the calyces as suggested by the electrophysiological data rather than in MNTB neurons.

Table 1. Comparison of PMCA2 function in *deafwaddler* mutants and DTR mice. The % of PMCA protein is calculated based on the number of functional alleles possessed by an animal, assuming that all alleles produce the same amount of protein. Due to the premature stop codon in the dfw2J mutation, no protein is produced. The efficiency of PMCA2 was calculated by Penheiter and colleagues using a calcium clearance assay in the dfw mutants (Penheiter et al. 2001). In +/dfw2J heterozygotes the efficiency of the existing PMCA will be wild type like, but its overall function in the animal only amounts to 50%.

References

Ashmore J, and Gale J. The cochlea. *Current biology : CB* 10: R325-327, 2000.

Attwell D, and Laughlin SB. An energy budget for signaling in the grey matter of the brain. *Journal of cerebral blood flow and metabolism : official journal of the International Society of Cerebral Blood Flow and Metabolism* 21: 1133-1145, 2001.

Billups B, and Forsythe ID. Presynaptic mitochondrial calcium sequestration influences transmission at mammalian central synapses. *The Journal of neuroscience : the official journal of the Society for Neuroscience* 22: 5840-5847, 2002.

Bollmann JH, Sakmann B, and Borst JG. Calcium sensitivity of glutamate release in a calyx-type terminal. *Science* 289: 953-957, 2000.

Borst JG, Helmchen F, and Sakmann B. Pre- and postsynaptic whole-cell recordings in the medial nucleus of the trapezoid body of the rat. *The Journal of physiology* 489 (Pt 3): 825-840, 1995.

Brini M, Di Leva F, Domi T, Fedrizzi L, Lim D, and Carafoli E. Plasma-membrane calcium pumps and hereditary deafness. *Biochemical Society transactions* 35: 913-918, 2007.

Corwin JT, and Warchol ME. Auditory hair cells: structure, function, development, and regeneration. *Annual review of neuroscience* 14: 301-333, 1991.

Dumont RA, Lins U, Filoteo AG, Penniston JT, Kachar B, and Gillespie PG. Plasma membrane Ca2+-ATPase isoform 2a is the PMCA of hair bundles. *The Journal of neuroscience : the official journal of the Society for Neuroscience* 21: 5066-5078, 2001.

Felmy F, and Schneggenburger R. Developmental expression of the Ca2+-binding proteins calretinin and parvalbumin at the calyx of held of rats and mice. *The European journal of neuroscience* 20: 1473-1482, 2004.

Felmy F, and von Gersdorff H. Late switch for post-tetanic potentiation: once again it's Ca2+. Focus on "An increase in calcium influx contributes to post-tetanic potentiation at the rat calyx of Held synapse". *Journal of neurophysiology* 96: 2840-2841, 2006.

Ficarella R, Di Leva F, Bortolozzi M, Ortolano S, Donaudy F, Petrillo M, Melchionda S, Lelli A, Domi T, Fedrizzi L, Lim D, Shull GE, Gasparini P, Brini M, Mammano F, and Carafoli E. A functional study of plasma-membrane calcium-pump isoform 2 mutants causing digenic deafness. *Proceedings of the National Academy of Sciences of the United States of America* 104: 1516-1521, 2007.

Flores-Otero J, and Davis RL. Synaptic proteins are tonotopically graded in postnatal and adult type I and type II spiral ganglion neurons. *The Journal of comparative neurology* 519: 1455-1475, 2011.

Franzen DL, Gleiss SA, Berger C, Kumpfbeck FS, Ammer JJ, and Felmy F. Development and modulation of intrinsic membrane properties control the temporal precision of auditory brain stem neurons. *Journal of neurophysiology* 113: 524-536, 2015.

Gazula VR, Strumbos JG, Mei X, Chen H, Rahner C, and Kaczmarek LK. Localization of Kv1.3 channels in presynaptic terminals of brainstem auditory neurons. *The Journal of comparative neurology* 518: 3205-3220, 2010.

Golub JS, Tong L, Ngyuen TB, Hume CR, Palmiter RD, Rubel EW, and Stone JS. Hair cell replacement in adult mouse utricles after targeted ablation of hair cells with diphtheria toxin. *The Journal of neuroscience : the official journal of the Society for Neuroscience* 32: 15093-15105, 2012.

Guinan JJ, Jr., and Li RY. Signal processing in brainstem auditory neurons which receive giant endings (calyces of Held) in the medial nucleus of the trapezoid body of the cat. *Hearing research* 49: 321-334, 1990.

Kochubey O, Han Y, and Schneggenburger R. Developmental regulation of the intracellular Ca2+ sensitivity of vesicle fusion and Ca2+-secretion coupling at the rat calyx of Held. *The Journal of physiology* 587: 3009-3023, 2009.

Kopp-Scheinpflug C, Lippe WR, Dorrscheidt GJ, and Rubsamen R. The medial nucleus of the trapezoid body in the gerbil is more than a relay: comparison of pre- and postsynaptic activity. *Journal of the Association for Research in Otolaryngology : JARO* 4: 1-23, 2003.

Kopp-Scheinpflug C, Tolnai S, Malmierca MS, and Rubsamen R. The medial nucleus of the trapezoid body: comparative physiology. *Neuroscience* 154: 160-170, 2008.

Kozel PJ, Davis RR, Krieg EF, Shull GE, and Erway LC. Deficiency in plasma membrane calcium ATPase isoform 2 increases susceptibility to noise-induced hearing loss in mice. *Hearing research* 164: 231-239, 2002.

Kozel PJ, Friedman RA, Erway LC, Yamoah EN, Liu LH, Riddle T, Duffy JJ, Doetschman T, Miller ML, Cardell EL, and Shull GE. Balance and hearing deficits in mice with a null mutation in the gene encoding plasma membrane Ca2+-ATPase isoform 2. *The Journal of biological chemistry* 273: 18693-18696, 1998.

Leao RN, Sun H, Svahn K, Berntson A, Youssoufian M, Paolini AG, Fyffe RE, and Walmsley B. Topographic organization in the auditory brainstem of juvenile mice is disrupted in congenital deafness. *The Journal of physiology* 571: 563-578, 2006.

Lippe WR. Rhythmic spontaneous activity in the developing avian auditory system. *The Journal of neuroscience : the official journal of the Society for Neuroscience* 14: 1486-1495, 1994.

Lorteije JA, Rusu SI, Kushmerick C, and Borst JG. Reliability and precision of the mouse calyx of Held synapse. *The Journal of neuroscience : the official journal of the Society for Neuroscience* 29: 13770-13784, 2009.

Mahrt EJ, Perkel DJ, Tong L, Rubel EW, and Portfors CV. Engineered deafness reveals that mouse courtship vocalizations do not require auditory experience. *The Journal of neuroscience : the official journal of the Society for Neuroscience* 33: 5573-5583, 2013.
McCullough BJ, Adams JC, Shilling DJ, Feeney MP, Sie KC, and Tempel BL. 3p-- syndrome defines a hearing loss locus in 3p25.3. *Hearing research* 224: 51-60, 2007.
McCullough BJ, and Tempel BL. Haplo-insufficiency revealed in deafwaddler mice when tested for hearing loss and ataxia. *Hearing research* 195: 90-102, 2004.
Muller M, Goutman JD, Kochubey O, and Schneggenburger R. Interaction between facilitation and depression at a large CNS synapse reveals mechanisms of short-term plasticity. *The Journal of neuroscience : the official journal of the Society for Neuroscience* 30: 2007-2016, 2010.
Pasic TR, Moore DR, and Rubel EW. Effect of altered neuronal activity on cell size in the medial nucleus of the trapezoid body and ventral cochlear nucleus of the gerbil. *The Journal of comparative neurology* 348: 111-120, 1994.
Pasic TR, and Rubel EW. Cochlear nucleus cell size is regulated by auditory nerve electrical activity. *Otolaryngology--head and neck surgery : official journal of American Academy of Otolaryngology-Head and Neck Surgery* 104: 6-13, 1991.
Pasic TR, and Rubel EW. Rapid changes in cochlear nucleus cell size following blockade of auditory nerve electrical activity in gerbils. *The Journal of comparative neurology* 283: 474-480, 1989.
Penheiter AR, Filoteo AG, Croy CL, and Penniston JT. Characterization of the deafwaddler mutant of the rat plasma membrane calcium-ATPase 2. *Hearing research* 162: 19-28, 2001.
Rubel EW. Ontogeny of Structure and Function in the Vertebrate Auditory System. In: *Handbook of Sensory Physiology, Vol IX, Development of Sensory Systems*, edited by Jacobson M., Springer-Verlag, 1978, p. 135-237.
Schneggenburger R, and Forsythe ID. The calyx of Held. *Cell and tissue research* 326: 311-337, 2006.
Schultz JM, Yang Y, Caride AJ, Filoteo AG, Penheiter AR, Lagziel A, Morell RJ, Mohiddin SA, Fananapazir L, Madeo AC, Penniston JT, and Griffith AJ. Modification of human hearing loss by plasma-membrane calcium pump PMCA2. *The New England journal of medicine* 352: 1557-1564, 2005.
Sengupta B, Faisal AA, Laughlin SB, and Niven JE. The effect of cell size and channel density on neuronal information encoding and energy efficiency. *Journal of cerebral blood flow and metabolism : official journal of the International Society of Cerebral Blood Flow and Metabolism* 33: 1465-1473, 2013.
Smith DJ, and Rubel EW. Organization and development of brain stem auditory nuclei of the chicken: dendritic gradients in nucleus laminaris. *The Journal of comparative neurology* 186: 213-239, 1979.
Sonntag M, Englitz B, Kopp-Scheinpflug C, and Rubsamen R. Early postnatal development of spontaneous and acoustically evoked discharge activity of principal cells of the medial nucleus of the trapezoid body: an in vivo study in mice. *The Journal of neuroscience : the official journal of the Society for Neuroscience* 29: 9510-9520, 2009.
Street VA, McKee-Johnson JW, Fonseca RC, Tempel BL, and Noben-Trauth K. Mutations in a plasma membrane Ca2+-ATPase gene cause deafness in deafwaddler mice. *Nature genetics* 19: 390-394, 1998.
Takahashi K, and Kitamura K. A point mutation in a plasma membrane Ca(2+)-ATPase gene causes deafness in Wriggle Mouse Sagami. *Biochemical and biophysical research communications* 261: 773-778, 1999.
Taschenberger H, and von Gersdorff H. Fine-tuning an auditory synapse for speed and fidelity: developmental changes in presynaptic waveform, EPSC kinetics, and synaptic plasticity. *The Journal of neuroscience : the official journal of the Society for Neuroscience* 20: 9162-9173, 2000.
Tilney MS, Tilney LG, and DeRosier DJ. The distribution of hair cell bundle lengths and orientations suggests an unexpected pattern of hair cell stimulation in the chick cochlea. *Hearing research* 25: 141-151, 1987.

Tollin DJ. The lateral superior olive: a functional role in sound source localization. *The Neuroscientist : a review journal bringing neurobiology, neurology and psychiatry* 9: 127-143, 2003.

Tong H, Kopp-Scheinpflug C, Pilati N, Robinson SW, Sinclair JL, Steinert JR, Barnes-Davies M, Allfree R, Grubb BD, Young SM, Jr., and Forsythe ID. Protection from Noise-Induced Hearing Loss by Kv2.2 Potassium Currents in the Central Medial Olivocochlear System. *The Journal of neuroscience : the official journal of the Society for Neuroscience* 33: 9113-9121, 2013.

Tong L, Strong MK, Kaur T, Juiz JM, Oesterle EC, Hume C, Warchol ME, Palmiter RD, and Rubel EW. Selective deletion of cochlear hair cells causes rapid age-dependent changes in spiral ganglion and cochlear nucleus neurons. *The Journal of neuroscience : the official journal of the Society for Neuroscience* 35: 7878-7891, 2015.

Tritsch NX, Rodriguez-Contreras A, Crins TT, Wang HC, Borst JG, and Bergles DE. Calcium action potentials in hair cells pattern auditory neuron activity before hearing onset. *Nature neuroscience* 13: 1050-1052, 2010.

von Gersdorff H, and Borst JG. Short-term plasticity at the calyx of held. *Nature reviews Neuroscience* 3: 53-64, 2002.

von Hehn CA, Bhattacharjee A, and Kaczmarek LK. Loss of Kv3.1 tonotopicity and alterations in cAMP response element-binding protein signaling in central auditory neurons of hearing impaired mice. *The Journal of neuroscience : the official journal of the Society for Neuroscience* 24: 1936-1940, 2004.

Wang LY, Gan L, Forsythe ID, and Kaczmarek LK. Contribution of the Kv3.1 potassium channel to high-frequency firing in mouse auditory neurones. *The Journal of physiology* 509 (Pt 1): 183-194, 1998.

Wang Y, Cunningham DE, Tempel BL, and Rubel EW. Compartment-specific regulation of plasma membrane calcium ATPase type 2 in the chick auditory brainstem. *The Journal of comparative neurology* 514: 624-640, 2009.

Yamoah EN, Lumpkin EA, Dumont RA, Smith PJ, Hudspeth AJ, and Gillespie PG. Plasma membrane Ca2+-ATPase extrudes Ca2+ from hair cell stereocilia. *The Journal of neuroscience : the official journal of the Society for Neuroscience* 18: 610-624, 1998.

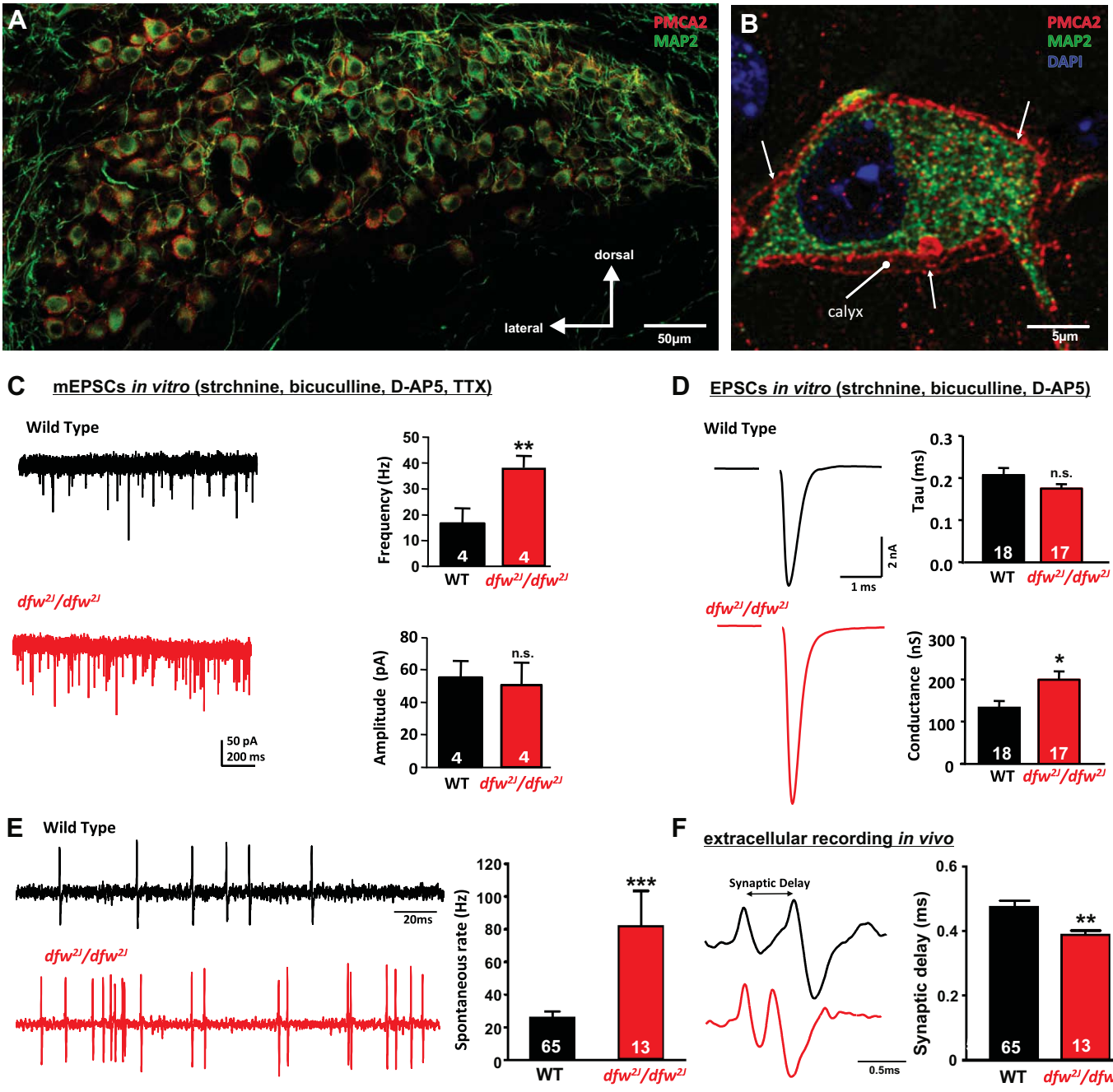
A
PMCA2
MAP2
dorsal
lateral
50µm
B
PMCA2
MAP2
DAPI
calyx
5µm
C
mEPSCs in vitro (strchnine, bicuculline, D-AP5, TTX)
Wild Type
dfw2J/dfw2J
50 pA
200 ms
Frequency (Hz)
Amplitude (pA)
n.s.
WT
dfw2J/dfw2J
D
EPSCs in vitro (strchnine, bicuculline, D-AP5)
Wild Type
2 nA
1 ms
Tau (ms)
Conductance (nS)
E
Wild Type
20ms
Spontaneous rate (Hz)
F
extracellular recording in vivo
Synaptic Delay
0.5ms
Synaptic delay (ms)

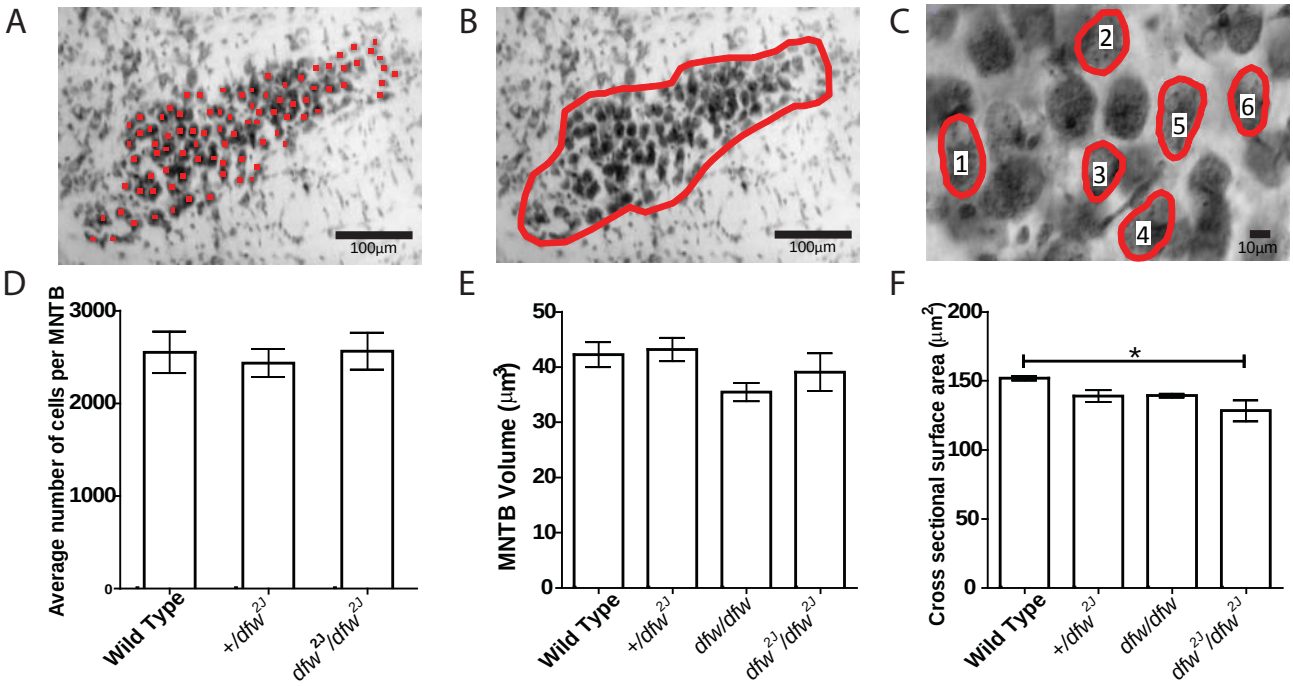
A
100µm
B
100µm
C
1
2
3
4
5
6
10µm
D
Average number of cells per MNTB
3000
2000
1000
0
Wild Type
+/dfw2J
dfw2J/dfw2J
E
MNTB Volume (µm3)
50
40
30
20
10
0
Wild Type
+/dfw2J
dfw/dfw
dfw2J/dfw2J
F
Cross sectional surface area (µm2)
200
150
100
50
0
*
Wild Type
+/dfw2J
dfw/dfw
dfw2J/dfw2J

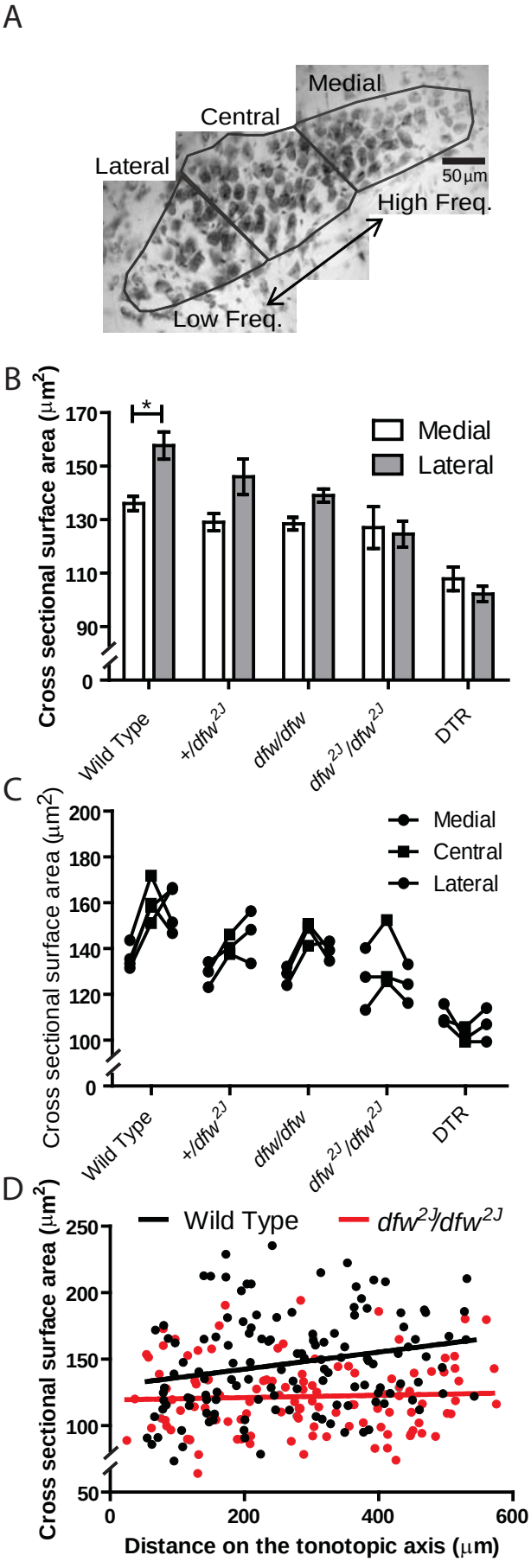
A
Medial
Central
Lateral
50 µm
High Freq.
Low Freq.
B
Cross sectional surface area (µm2)
170
150
130
110
90
0
*
Medial
Lateral
Wild Type
+/dfw2J
dfw/dfw
dfw2J/dfw2J
DTR
C
Cross sectional surface area (µm2)
200
180
160
140
120
100
0
Medial
Central
Lateral
Wild Type
+/dfw2J
dfw/dfw
dfw2J/dfw2J
DTR
D
Cross sectional surface area (µm2)
250
200
150
100
50
Wild Type
dfw2J/dfw2J
0
200
400
600
Distance on the tonotopic axis (µm)

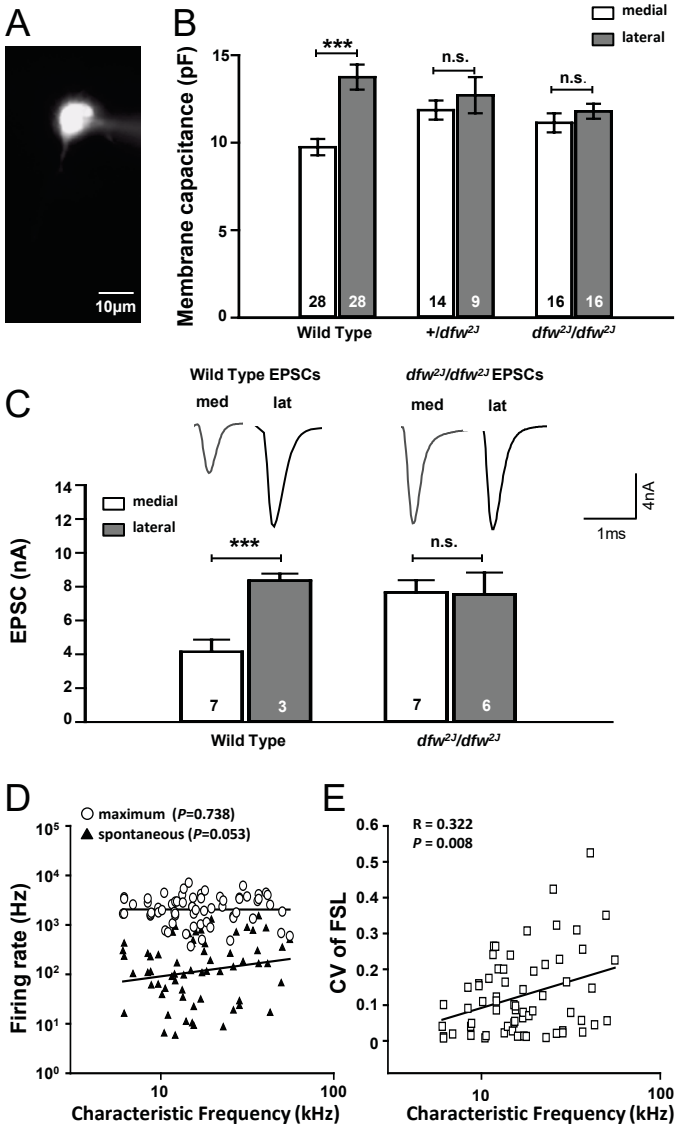
A
10μm
B
medial
lateral
Membrane capacitance (pF)
***
n.s.
n.s.
28
28
14
9
16
16
Wild Type
+/dfw2J
dfw2J/dfw2J
C
Wild Type EPSCs
dfw2J/dfw2J EPSCs
med
lat
med
lat
4nA
1ms
EPSC (nA)
medial
lateral
***
n.s.
7
3
7
6
Wild Type
dfw2J/dfw2J
D
maximum (P=0.738)
spontaneous (P=0.053)
Firing rate (Hz)
Characteristic Frequency (kHz)
E
R = 0.322
P = 0.008
CV of FSL
Characteristic Frequency (kHz)

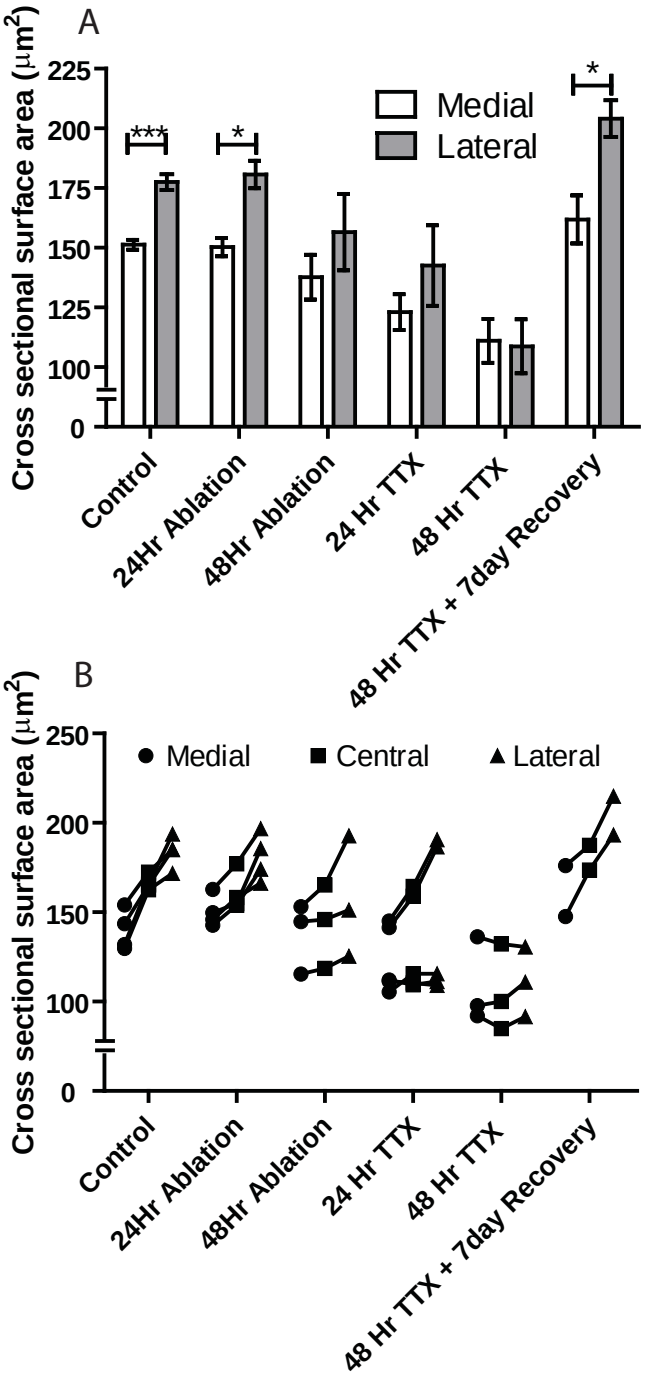
A
Cross sectional surface area (μm²)
225
200
175
150
125
100
0
Medial
Lateral
***
*
*
Control
24Hr Ablation
48Hr Ablation
24 Hr TTX
48 Hr TTX
48 Hr TTX + 7day Recovery
B
Cross sectional surface area (μm²)
250
200
150
100
0
Medial
Central
Lateral
Control
24Hr Ablation
48Hr Ablation
24 Hr TTX
48 Hr TTX
48 Hr TTX + 7day Recovery

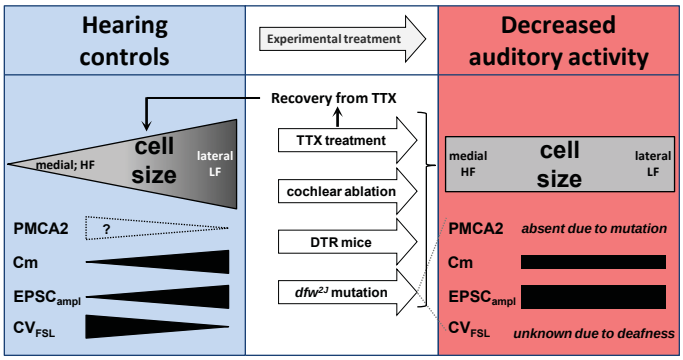
Hearing controls
Experimental treatment
Decreased auditory activity
Recovery from TTX
TTX treatment
cochlear ablation
DTR mice
dfw2J mutation
medial; HF
cell size
lateral LF
PMCA2
?
Cm
EPSCampl
CVFSL
medial HF
cell size
lateral LF
PMCA2
absent due to mutation
Cm
EPSCampl
CVFSL
unknown due to deafness

Genotype	Hearing phenotype	PMCA Protein	PMCA Efficiency	PMCA Function
Wildtype	normal	100%	100%	100%
+/dfw^{2J}	High frequency loss	~50%	100%	~50%
dfw/dfw	deaf	100%	~30%	~30%
dfw^{2J}/dfw^{2J}	deaf	0%	0%	0%
DTR	deaf	100%	100%	100%